Scaling behavior and complexity of plastic deformation for a bulk metallic glass at cryogenic temperatures

Cun Chen, Jingli Ren, Gang Wang, Karin A. Dahmen, and Peter K. Liaw

Phys. Rev. E **92**, 012113 — Published 8 July 2015

DOI: 10.1103/PhysRevE.92.012113

Scaling Behavior and Complexity of Plastic Deformation for a Bulk Metallic Glass at Cryogenic Temperatures

Cun Chen[1], Jingli Ren[1, a)], Gang Wang[2], Karin A. Dahmen[3], and Peter K. Liaw[4]

[1]School of Mathematics and Statistics, Zhengzhou University, 100 Science Road, Zhengzhou 450001, China

[2]Laboratory for Microstructures, Shanghai University, Shanghai 200444, China

[3]Department of Physics and Institute of Condensed Matter Theory, University of Illinois at Urbana Champaign, 1110 West Green Street, Urbana, IL 61801, USA

[4]Department of Materials Science and Engineering, The University of Tennessee, Knoxville, TN 37996 USA

[a)] Corresponding authors: renjl@zzu.edu.cn

Abstract

We explore the scaling behavior and complexity in the shear-branching process during the compressive deformation of a bulk metallic glass (BMG), $Zr_{64.13}Cu_{15.75}Al_{10}Ni_{10.12}$ (at. %) at cryogenic temperatures. The fractal dimension of the stress rate signal ranges from 1.22 to 1.72 with decreasing temperature, and a larger shear-branching rate occurs at lower temperature. A stochastic model is introduced for the shear-branching process. Especially, at the temperature of 213 K, the shear-branching process evolves as a self-similar random process. In addition, the complexity of the stress rate signal conforms to the larger activation energy of the shear transformation zone at lower temperatures.

PACS: 02.50.Fz; 05.45.Df; 81.05.Kf; 62.20.fk

To explore the plastic deformation mechanism during compressive deformation for bulk metallic glasses (BMGs), the serrated flow signal is usually discussed by various methods, such as the chaotic time series analysis [1], the statistical analysis [1-4], and the spatio-temporal dynamic model [5-8]. Shear-band-slip avalanche is the dominant mechanism of plastic deformation in BMGs, which demonstrates the agreement between high temporal resolution measurements of the slip statistics, and the dynamics with the predictions of a simple mean-field theory [9, 10]. The multiple shear-band patterns show fractal characteristics in the severely deformed BMGs under specific loading conditions [11]. For the BMGs with good ductility, the dynamics of the serrated plastic flow manifests a self-organization critical (SOC) state, which has a power-law scaling behavior [1].

Recently, a few of studies focus on the deformation behavior of BMGs under extreme conditions, such as at cryogenic temperatures or high strain rates [12-16]. The shear-banding behavior and the plastic flow for the inhomogeneous deformation of BMGs are considered to be affected by deformation units [14]. The activation energy increment of the deformation units at lower temperatures is the main factor influencing the fracture strength of BMGs [17]. In fact, the plasticity of BMGs is unexpectedly improved with decreasing temperature [4, 12]. However, the exact elucidation of how the temperature influences the plastic deformation of BMGs is still unclear. In the current work, the scale-free fractal behavior, and the complexity information in the shear-branching process of a BMG is investigated to provide valuable information to further characterize the evolution of the shear bands and plastic deformation mechanism of BMGs at cryogenic temperatures, since the intermittent serrated flow is not appropriate for the continuous system, and the stress-time signal of metallic glasses appears quite complicatedly and irregularly.

A $Zr_{64.13}Cu_{15.75}Al_{10}Ni_{10.12}$ (at. %) BMG is compressed at a temperature ranges from 133 K to 305 K with a strain rate of 2.5×10^{-4} s^{-1}. The stress-time curves are established in Fig. 1, which shows that as the temperature decreases from 305 K to 133 K, the amplitude of serrations reduces gradually, and disappears at the temperature of 193 K. Clearly, there is a transition from the serrated to non-serrated

plastic flow with decreasing temperature. Hence, it is required to investigate the plastic deformation mechanism not only based on the serrated flow but also based on the non-serrated flow.

It was shown in previous works [18-21] that some degrees of short- and medium-range order did exist in BMGs, which means there are self-similarity characteristics hidden in BMGs. Xi *et al*. found a fractal-like dimpled structure on the fracture surface of a Ti-based BMG [22]. Afterwards, Sun *et al*. further quantitatively analyzed the fractal characteristic on the 2-dimension fracture surface of Zr-based BMG [11]. The analysis based on the 2-dimension fracture surface reflects the local feature of the shear-branching process for which actually spread in a 3-dimension space. Considering that the measurement of shear bands distributed spatially is difficult to be achieved, we focus our research on the temporal stress rate signal of $Zr_{64.13}Cu_{15.75}Al_{10}Ni_{10.12}$ BMG, $\{\mathrm{d}\sigma(i)/\mathrm{d}t, i=1,2,\cdots,N\}$ (see Fig. 2), because it reflects the global feature of the shear-branching process.

The calculation of the fractal dimension is according to the box-counting method [23] based on the stress rate signal, $\{x(i)=\mathrm{d}\sigma(i)/\mathrm{d}t, i=1,2,\cdots,N\}$. Square boxes with a length of l can cover the total data set, which needs at least $N(l)$ boxes. Changing the box size, l, we can obtain a series of $N(l)$. Fitting (l, $N(l)$) in a double logarithmic plot, the slope of this fitting curve is expressed as,

$$D=-\lim_{l\to 0}\frac{\log N(l)}{\log l} \quad , \tag{1}$$

where D is the fractal dimension of stress rate signal.

The fractal dimension, D, as a function of the temperature is plotted in Fig. 3. It can be seen that the D value increases with decreasing the temperature from 305 K to 133 K, suggesting an enhanced fractal behavior at low temperature. The largest D value appears at the temperature of 133 K, indicating the largest shear-branching rate. In this case, numerous shear bands with hierarchical structure can propagate in a scale-free manner. The fractal dimension of the shear-branching structure actually reflects the branching rates of a primary shear band evolving to the secondary shear

band. The formation of the fractal structure is resulted from the interactions among shear-band hierarchies located at different places and directions. For BMGs at lower temperatures with a larger fractal dimension, the plasticity is also improved, which is attributed to the concurrent nucleation of a large number of shear bands throughout the sample. The higher density of shear bands in turn can induce a hierarchical structure in the length scales of shear banding. Thus, a large number of shear bands usually are accompanied by the spread of the hierarchical structure. The shear-branching process include short-range interactions from the intersection of the shear bands, the consequent arrest, and long-range interaction of the strain fields initiated from different shear bands. Along with the shear-branching process, the serrated flow behavior is manifested in the plastic regime in the Zr-based BMG. Each stress drop in the serration event corresponds to the system surmounting the barrier, and then jumping to a neighboring metastable state, which was believed to behave a self-organization critical (SOC-type) dynamics, especially at lower temperatures (cryogenic level) [4].

Based on the stress rate signal, $\{x(i) = \mathrm{d}\sigma(i)/\mathrm{d}t, i = 1,2,\cdots,N\}$, the detrended fluctuation analysis is used to quantify the evolution of the shear-branching structure. The process of the detrended fluctuation analysis is described as following [24-27]. Divide the signal $\{x(i), i = 1,2,\cdots,N\}$ into N_q (where $N_q = N/q$) zones with each zone containing q elements. In the k-th zone, the local trend is defined as a linear function of $\hat{x}_k(j)$, $j = 1,2,\cdots,q$, which is linearly fitted by the original series, $x_k(j), j = 1,2,\cdots,q$. The detrended time series is, $x_k(j) - \hat{x}_k(j), j = 1,2,\cdots,q$, with a mean-square error, $F^2(k) = \frac{1}{q}\sum_{j=1}^{q}(x_k(j) - \hat{x}_k(j))^2$. The root-mean-square is expressed as, $F_q = (\frac{1}{N_q}\sum_{k=1}^{N_q} F^2(k))^{\frac{1}{2}}$, in the total N_q zones. F_q is a power function of the scale, q, $F_q \sim q^H$, where H is the Hurst exponent reflecting the long-range memory dependence of the signal.

According to the above detrended fluctuation analysis, the Hurst exponent, *H,* vs. temperature is shown in Fig. 3. The Hurst exponent, *H*, ranges from 0.11 to 0.48 (see Table.1). Here $H \in (0, 0.5)$ means a negative correlation and an anti-persistent process during the shear-branching process, which implies the evolution trend of shear-branching is opposite to the past progress due to the absence of the long-memory dependence. The stress rate increases persistently in a period of time, and then decreases in the next period of time. This trend is consistent with that of the serrated flow, which increases during the elastic energy aggregation, and then decreases during the energy release.

As the temperature decreases, Hurst exponent increases to the maximum value of 0.48 at 213 K and then decreases (see Fig. 3). The maximum Hurst exponent at 213 K reflects that the stress rate signal is a self-similar random process with a weak negative correlation. The shear-branching process behaves a random walk, which induces a homogenization in some degrees. On the other hand, the small *H* value (such as H = 0.11 at 133 K) means a strong negative correlation of the shear-branching process. This strong anti-persistent behavior is accompanied with increasing the hybridization of shear bands. In this case, the deformation caused by multiple interactions between shear bands is characterized by a low degree of homogenization, i.e., heterogeneity.

An inner correlation between the fractal dimension and Hurst exponent can be described by the modified Cauchy class [28], as a stochastic process. The modified Cauchy class consists of a stationary Gaussian random processes, $Z(x)$, $x \in R$, which are characterized by their correlation function, $c(r) = < Z(x), Z(x+r) >$, $x \in R$, and a correlation function satisfying $c(r) = (1+|r|^{\alpha})^{-(\beta/\alpha)-1}(1+(1-\beta)|r|^{\alpha})$, $r \in R$, where $\alpha \in (0, 2]$, $\beta > 1$. The fractal dimension, *D*, is given by $D = n+1-\alpha/2$, and the Hurst exponent, *H*, given by $H = 1-\beta/2$. Considering the result that we calculated here, $H \in (0, 0.5)$, we give the restriction of $\beta > 1$ in the modified Cauchy class, which can feature the negative correlation of the signal.

The stochastic model is suitable for the current situation because not all of the D and H conform to the linear relationship, i. e., $D + H = 2$, see Fig. 3 (The curve of $D + H$ vs. temperature). Especially, at the temperature of 213 K, the value of $D + H$ is equal to 1.88 (approximately equal to 2), which suggest that the signal is more close to a self-similar random process. This result is consistent with the above analysis that Hurst exponent $H = 0.48$ at 213 K, reflecting that the stress rate signal is a self-similar random process with a weak negative correlation. In addition, from Fig. 2, we observe that the signal, $\{\mathrm{d}\sigma(i)/\mathrm{d}t, i = 1,2,\cdots,N\}$, is smoothed as the Hurst exponent increases. The tendency here is consistent with the identification of the modified Cauchy class: the more close to 0.5 of the Hurst exponent, the smoother of the signal curve [28].

To further characterize the complexity of the system, the concept of entropy is introduced. We can obtain the accurate result about the system by the approximate entropy (*ApEn*) method [29]. The calculated value of *ApEn* is shown in Table. 1, and the *ApEn* as a function of temperature is presented in Fig. 4. A large value of *ApEn* plotted at low temperature range suggests the stress rate signal exhibiting a high complexity, which is consistent with the above fractal analysis, and the detrended fluctuation analysis. A large fractal dimension at low temperatures reflects the high shear-branching rate with a complex hierarchical structure. A small Hurst exponent (i.e., a strong negative correlation) reflects a low degree of homogenization. The heterogeneity in stress rate signal induces a disordered and complicated shear-branching process, which can also be observed from the fracture surface.

The activation energy $W = (8/\pi^2)\gamma_C^2 G\Omega$, where G is the shear modulus, Ω is the effective shear transition zone (STZ) volume, and γ_c is a critical shear strain for BMGs ($\gamma_c = 0.036$ is found to be a constant for BMGs at room temperature) [30]. The activation volume of STZ can be calculated by the formula $\Omega = \dfrac{kT\ln(\omega_0/C\dot{\gamma})}{4RG_{0T}\gamma_C^2\varsigma(1-\tau_{CT}/\tau_{C0})^{3/2}}$ [31], where $\ln(\omega_0/C\dot{\gamma}) \approx 30$, $R \approx 0.25$, $\varsigma \approx 3$; T is the environmental temperature, k is Boltzmann constant (1.381×10^{-23} J/K), τ_{C0} is the

yield shear stress at 0 K (τ_{C0} = 1124 MPa), G_{0T} is the shear modulus at the temperature of T (G_{0T} =31.2 GPa); The critical shear stress τ_{CT} satisfies, $\tau_{CT}/G = \gamma_{C0} - \gamma_{C1}(T/T_g)^{2/3}$, where γ_{C0} = 0.036, γ_{C1} = 0.016. The necessary mechanical properties of the $Zr_{64.13}Cu_{15.75}Al_{10}Ni_{10.12}$ BMG compressed at different temperatures are shown in Table. 2. Based on the above information, the volume and activation energy of STZ can be calculated (see Fig. 5). The volume of STZ increases as temperatures decreasing from 305 K to 133 K, the activation energy of STZ increases correspondingly. This result is consistent with the calculation results of the *ApEn* value, i.e., a more complexity of the shear-branching process appearing at low temperature. The larger fractal dimension reflects a more complex hierarchical structure of the shear-branching process at lower temperatures. The high complexity of the shear-branching process at low temperature confirms theoretically that there is a large activation energy used for activating the STZ, which facilitates the plastic flow of BMGs.

In summary, the self-similar behavior and complexity in the temporal scale of the stress rate signal are investigated at temperatures well below the glass-transition temperature. The obvious fractal behavior suggests that the shear-banding process is accompanied with larger branching rates from a primary shear band to a secondary shear band. In fact, at the temperature of 133 K, there is a large amount of shear-band interacting with each other and more elastic energy that the sample contains, which is facilitated to produce the good plasticity of metallic glasses. A Cauchy class model is introduced for the stochastic shear-branching process, which connects the fractal dimension and Hurst exponent, as well as features the negative correlation process. In addition, the Hurst exponent reaches the maximum value of 0.48 at temperature of 213 K; especially, at the temperature of 213 K, the value of $D + H$ approaches 2, suggesting the shear-branching process evolves as a self-similar random process, which induced a degree of homogenization in shear bands. Furthermore, the analysis of approximate entropy suggests there is complicated hierarchy structure at low temperatures, which can be interpreted as, at the lower temperatures there are large

amounts of shear bands interacting which induced to SOC state. We give an explanation of the super plasticity of the BMGs from the perspective of the temporal scaling behavior and complexity at low temperature.

Acknowledgements The work described in this paper is supported by the NSFC (Grants No. 11271339, No. 51171098, and No. 51222102), the ZDGD13001 program. PKL very much appreciates the financial support from the US National Science Foundation (CMMI-1100080) with C. V. Cooper as the contract monitor. KAD and PKL are very grateful for the support from the US Department of Energy (DOE), Office of Fossil Energy, National Energy Technology Laboratory (DE-FE-0008855, DE-FE-0011194, and DE-FE-0024054), and the US Army Research Office (W911NF-13-1-0438) with V. Cedro, J. Mullen, S. Markovich, R. Dunst, S. Mathaudhu, and D. Stepp as contract monitors.

References

[1] R. Sarmah, G. Ananthakrishna, B. A. Sun, and W. H. Wang, Acta Mater. **59**, 4482 (2011).

[2] G. Wang, K. C. Chan, L. Xia, P. Yu, J. Shen, and W. H. Wang, Acta Mater. **57**, 6146 (2009).

[3] J. L. Ren, C. Chen, G. Wang, N. Mattern, and J. Eckert, AIP advances **1**, 032158(2011).

[4] J. L. Ren, C. Chen, Z. Y. Liu, R. Li, and G. Wang, Phys. Rev. B. **86**, 134303 (2012).

[5] Y. Q. Cheng, Z. Han, Y. Li, and E. Ma, Phys. Rev. B. **80**, 134115 (2009).

[6] B. A. Sun, H. B. Yu, W. Jiao, H. Y. Bai, D. Q. Zhao, and W. H. Wang, Phys. Rev. Lett. **105**, 035501 (2010).

[7] B. A. Sun, S. Pauly, J. Tan, M. Stoica, W. H. Wang, U. Kühn, and J. Eckert, Acta.

Mater. **60**, 4160 (2012).

[8] J. L. Ren, C. Chen, G. Wang, W. S. Cheung, B. A. Sun, N. Mattern, S. Siegmund, and J. Eckert, J. Appl. Phys. **116**, 033520 (2014).

[9] J. Antonaglia, W. J. Wright, X. J. Gu, R. R. Byer, T. C. Hufnagel, M. LeBlanc, J. T. Uhl, and K. A. Dahmen, Phys. Rev. Lett. **112**, 155501(2014).

[10] J. Antonaglia, X. Xie, G. Schwarz, M. Wraith, J. W. Qiao, Y. Zhang, P. K. Liaw, J. T. Uhl, and K. A. Dahmen, Sci. Rep. **4**, 4382 (2014)

[11] B. A. Sun and W. H. Wang, Appl. Phys. Lett. **98**, 201902 (2011).

[12] Z. Y. Liu, G. Wang, K. C. Chan, J. L. Ren, Y. L. Huang, X. L. Bian, X. H. Xu, D. S. Zhang, Y. L. Gao, Q. J. Zhai, J. Appl. Phys. **114**, 033520 (2013).

[13] Z. Wang, B. A. Sun, H. Y. Bai, and W. H. Wang, Nat. Commun. **5**, 5823 (2014).

[14] W. H. Jiang, F. X. Liu, D. C. Qiao, H. Choo, and P. K. Liaw, J. Mater. Res. **21**, 6, (2006).

[15] D. Klaumünzer, R. Maaß, F. H. Dalla Torre, and J. F. Löffler, Appl. Phys. Lett. **96**, 061901 (2010).

[16] W. H. Jiang, G. J. Fan, F. X. Liu, G.Y. Wang, H. Choo, and P. K. Liaw, International Journal of Plasticity, **24**, 1, 16 (2008).

[17] J. Tan, G. Wang, Z. Y. Liu, J. Bednacik, Y. L. Gao, Q. J. Zhai, N. Mattern, and J. Eckert, Sci. Rep. **4**, 3897 (2014).

[18] D. B. Miracle, Nat. Mater. **3**, 697702 (2004).

[19] D. B. Miracle, Acta Mater. **54**, 43174336 (2006).

[20] H. W. Sheng, W. K. Luo, F. M. Alamgir, J. M. Bai, and E. Ma, Nature, **439**, 419-425 (2006).

[21] D. Ma, A. D. Stoica, and X. L.Wang. Nat. Mater. **8**, 30 (2009).

[22] X. K. Xi, D. Q. Zhao, M. X. Pan, W. H. Wang, Y. Wu, and J. J. Lewandowski. Phys. Rev. Lett. **94**, 125510 (2005).

[23] T. Vicsek, Fractal Growth Phenomena (World Scientific, Singapore, 1992).

[24] C. K. Peng, J. Mietus, J. M. Hausdorff, S. Havlin, H. E. Stanley, and A. L. Goldberger, Phys. Rev. Lett. **70**, 1343 (1993).

[25] C. K. Peng, S. V. Buldyrev, S. Havlin, M. Simons, H. E. Stanley, and A. L.

Goldberger, Phys. Rev. E, **49**, 1685 (1994).

[26] K. Hu, P. Ivanov, Z. Chen, P. Carpena and H. E. Stanley, Phys. Rev. E, **64**, 011114 (2001).

[27] Z. Chen, P. Ivanov, K. Hu and H. E. Stanley, Phys. Rev. E, **65**, 041107 (2002).

[28] T. Gneiting, M. Schlather, SIAM Review, **46**, 22, 269-282 (2004).

[29] S. M. Pincus. Proceedings of the National Academy of Sciences, **88**, 2297-2301 (1991).

[30] M. D. Demetriou, J. S. Harmon, M. Tao, G. Duan, K. Samwer, and W. L. Johnson, Phys. Rev. Lett. **97**, 065502 (2006).

[31] W. L. Johnson and K. Samwer, Phys. Rev. Lett. **95**, 195501 (2005).

Figure captions

Fig. 1 (Color). Comparative stress-time curves for $Zr_{64.13}Cu_{15.75}Al_{10}Ni_{10.12}$ glassy metal deformed at different temperatures, 133 K, 153 K, 173 K, 193 K, 213 K, 233 K, 253 K, 273 K and 305 K with a strain rate of 2.5×10^{-4} s^{-1}.

Fig. 2 (Color online). The plot of the stress rate signal, $d\sigma / dt$, curves for the $Zr_{64.13}Cu_{15.75}Al_{10}Ni_{10.12}$ glassy metal compressed at a strain rate of 2.5×10^{-4} s^{-1} at different temperatures, 133 K, 153 K, 173 K, 193 K, 213 K, 233 K, 253 K, 273 K and 305 K with a strain rate of 2.5×10^{-4} s^{-1} (For clearly observing the difference between each other, here we capture part of the overall data).

Fig. 3 (Color online). The fractal dimension, D ["the red (middle) line"], Hurst exponent, H ["the green (lower) line"], and $D + H$ ["the black (upper) line"] of the stress rate signals, $d\sigma / dt$, for the $Zr_{64.13}Cu_{15.75}Al_{10}Ni_{10.12}$ glassy metal compressed at a strain rate of 2.5×10^{-4} s^{-1} and at different temperatures, 133 K, 153 K, 173 K, 193 K, 213 K, 233 K, 253 K, 273 K and 305 K with strain rate of 2.5×10^{-4} s^{-1}.

Fig. 4 (Color online). The approximate entropy *ApEn* at different temperatures, 133 K, 153 K, 173 K, 193 K, 213 K, 233 K, 253 K, 273 K and 305 K with strain rate of 2.5×10^{-4} s^{-1}.

Fig. 5 (Color online). (a) The volume of STZ at different temperatures. (b) The activation energies at different temperatures, 133 K, 153 K, 173 K, 193 K, 213 K, 233 K, 253 K, 273 K and 305 K.

Table. 1 The fractal dimension, D, Hurst exponent, H, values of $D + H$, and $ApEn$ of the signal $\{\mathrm{d}\sigma(i)/\mathrm{d}t, i = 1, 2, \cdots, N\}$ at different temperatures, 133 K, 153 K, 173 K, 193 K, 213 K, 233 K, 253 K, 273 K and 305 K with strain rate of 2.5×10^{-4} s^{-1}.

Temperature	133	153	173	193	213	233	253	273	305
D	1.72	1.64	1.7	1.7	1.4	1.33	1.28	1.31	1.22
H	0.11	0.12	0.12	0.13	0.48	0.32	0.35	0.28	0.25
$D + H$	1.83	1.76	1.82	1.83	1.88	1.65	1.63	1.59	1.47
$ApEn$	1.25	1.2	1.3	1.35	0.77	0.21	0.19	0.24	0.48

Table 2 Mechanical properties of the metallic glass compressed at different temperatures. T is the temperature, G_{0T} is the shear modulus, and τ_{CT} is the critical shear stress.

T (K)	183	203	213	223	273	293
G_{0T} (GPa)	30.2	30.0	29.9	29.8	28.9	28.5
τ_{CT} (MPa)	1087	1080	1076	1073	1040	1026

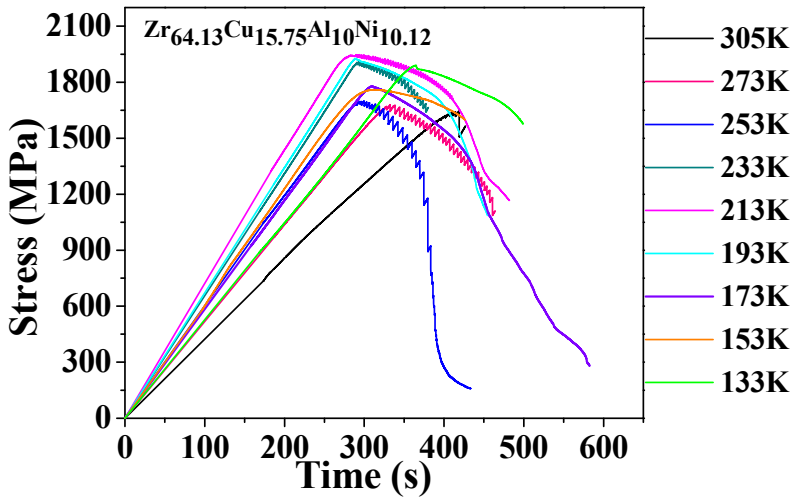
$Zr_{64.13}Cu_{15.75}Al_{10}Ni_{10.12}$
Stress (MPa)
Time (s)
0
300
600
900
1200
1500
1800
2100
0
100
200
300
400
500
600
305K
273K
253K
233K
213K
193K
173K
153K
133K

Fig. 1

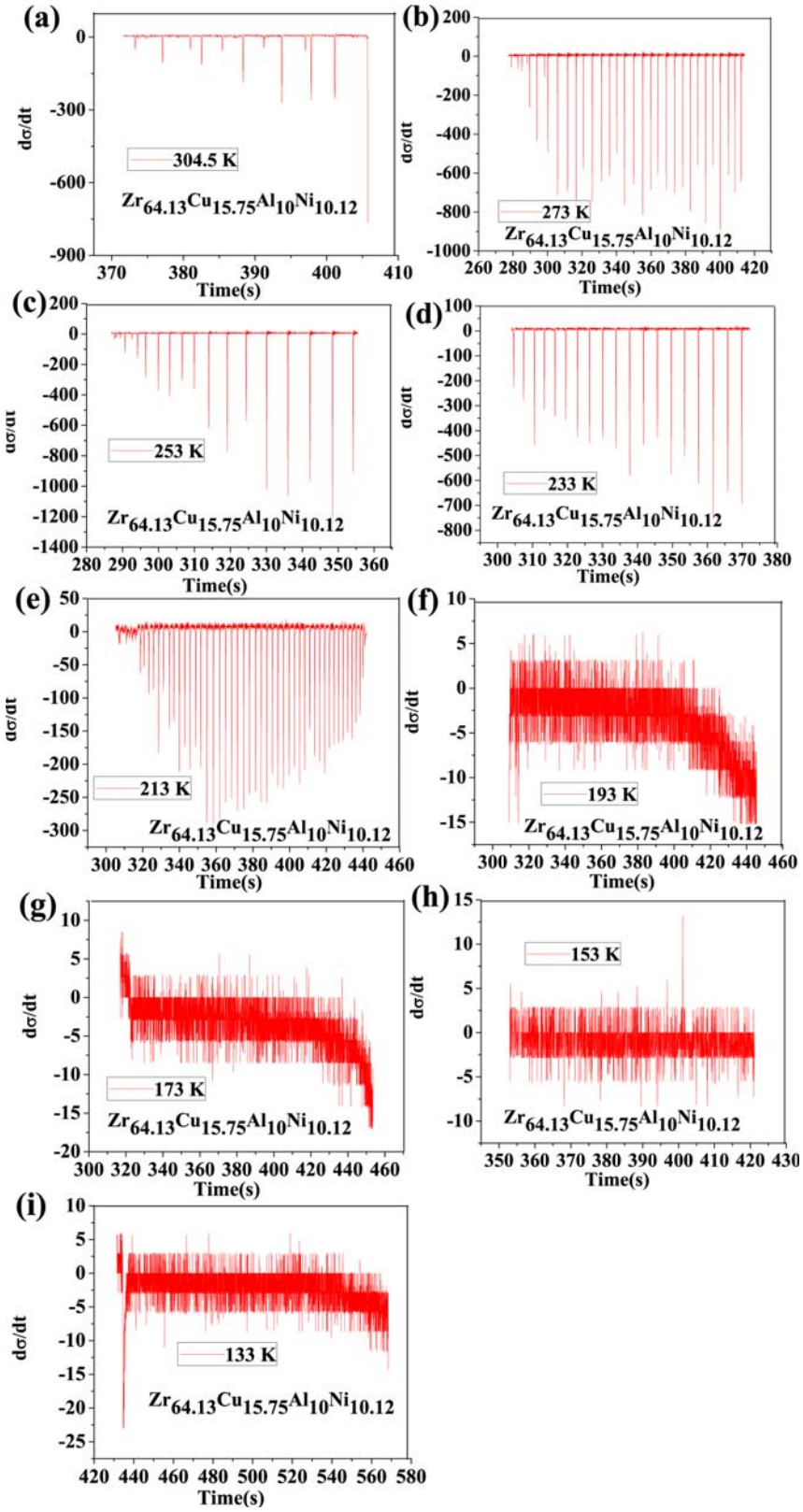
(a)
304.5 K
Zr64.13Cu15.75Al10Ni10.12
dσ/dt
Time(s)
(b)
273 K
Zr64.13Cu15.75Al10Ni10.12
dσ/dt
Time(s)
(c)
253 K
Zr64.13Cu15.75Al10Ni10.12
dσ/dt
Time(s)
(d)
233 K
Zr64.13Cu15.75Al10Ni10.12
dσ/dt
Time(s)
(e)
213 K
Zr64.13Cu15.75Al10Ni10.12
dσ/dt
Time(s)
(f)
193 K
Zr64.13Cu15.75Al10Ni10.12
dσ/dt
Time(s)
(g)
173 K
Zr64.13Cu15.75Al10Ni10.12
dσ/dt
Time(s)
(h)
153 K
Zr64.13Cu15.75Al10Ni10.12
dσ/dt
Time(s)
(i)
133 K
Zr64.13Cu15.75Al10Ni10.12
dσ/dt
Time(s)

Fig. 2

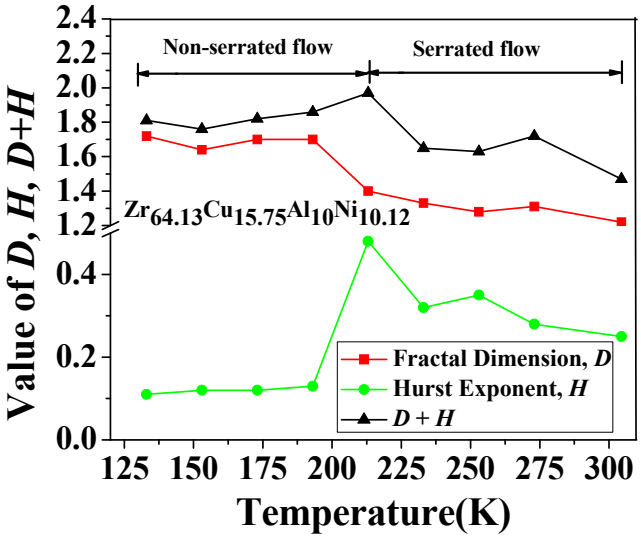
Non-serrated flow
Serrated flow
Zr64.13Cu15.75Al10Ni10.12
Fractal Dimension, D
Hurst Exponent, H
D + H
Value of D, H, D+H
Temperature(K)
2.4
2.2
2.0
1.8
1.6
1.4
1.2
0.4
0.2
0.0
125
150
175
200
225
250
275
300

Fig. 3

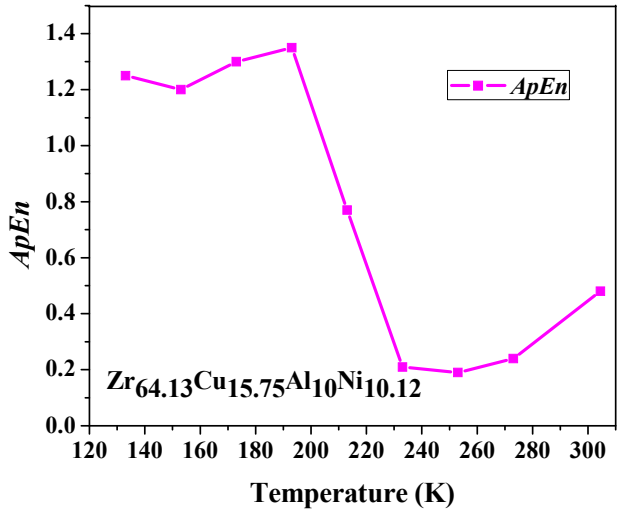
ApEn
1.4
1.2
1.0
0.8
0.6
0.4
0.2
0.0
120
140
160
180
200
220
240
260
280
300
Temperature (K)
ApEn
Zr64.13Cu15.75Al10Ni10.12

Fig. 4

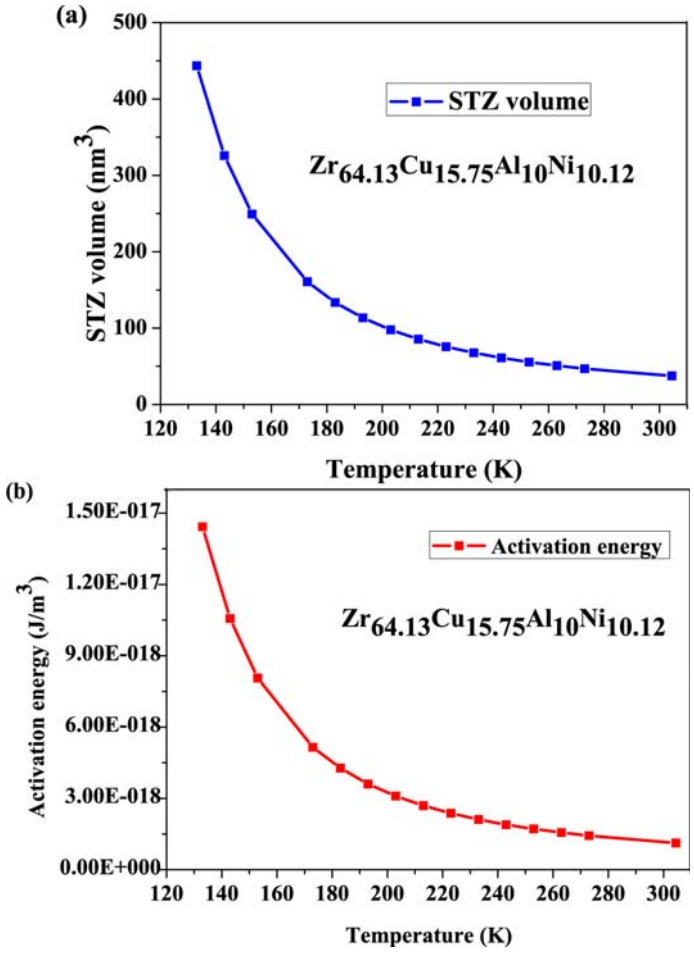
(a)
STZ volume
$Zr_{64.13}Cu_{15.75}Al_{10}Ni_{10.12}$
STZ volume (nm^3)
Temperature (K)
(b)
Activation energy
$Zr_{64.13}Cu_{15.75}Al_{10}Ni_{10.12}$
Activation energy (J/m^3)
Temperature (K)

Fig. 5